ARTICLES
PUBLISHED ONLINE: 3 NOVEMBER 2013 | DOI: 10.1038/NNANO.2013.221
nature nanotechnology

Optoelectronic control of surface charge and translocation dynamics in solid-state nanopores

Nicolas Di Fiori[1], Allison Squires[1], Daniel Bar[2], Tal Gilboa[2], Theodore D. Moustakas[3] and Amit Meller[1,2]*

Nanopores can be used to detect and analyse biomolecules. However, controlling the translocation speed of molecules through a pore is difficult, which limits the wider application of these sensors. Here, we show that low-power visible light can be used to control surface charge in solid-state nanopores and can influence the translocation dynamics of DNA and proteins. We find that laser light precisely focused at a nanopore can induce reversible negative surface charge densities as high as 1 C m^{-2}, and that the effect is tunable on submillisecond timescales by adjusting the photon density. By modulating the surface charge, we can control the amount of electroosmotic flow through the nanopore, which affects the speed of translocating biomolecules. In particular, a few milliwatts of green light can reduce the translocation speed of double-stranded DNA by more than an order of magnitude and the translocation speed of small globular proteins such as ubiquitin by more than two orders of magnitude. The laser light can also be used to unclog blocked pores. Finally, we discuss a mechanism to account for the observed optoelectronic phenomenon.

The manipulation of electrical surface charge in a rapid and reversible manner is important in a wide variety of biosensing applications, because electrostatic interactions influence the affinity and residence time of biological molecules in the sensing zone[1]. Charge manipulation in nanoscale sensors, such as nanopores, nanochannels and nanotubes[2–5], is particularly useful because of the scale of these devices. Solid-state nanopores are a prototypical class of nanoscale sensors that use electrophoretic forces to thread and translocate charged single nucleic acids or proteins through a nanoscale aperture in an ultrathin membrane[6–8]. The surface charge of a nanopore can affect its direct, Coulombic interactions with charged biomolecules, and can indirectly influence sensing by generating electroosmotic flow. This net flow can modulate the molecular capture rate[9] and molecular residence time in the sensing vicinity via hydrodynamic drag[10,11]. This effect has previously been characterized using optical tweezers[12] and by varying the zeta potential of a nanopore by changing the pH of the solution[13].

The ability to modulate the surface charge of a nanopore and, consequently, the associated electroosmotic flow, could allow the translocation speed of biomolecules to be controlled. This could in turn lead to the development of advanced single-molecule, low-cost characterization techniques for a broad spectrum of clinical samples, including genomic DNA, RNAs and proteins[14]. This challenge must be met without compromising the ability of the sensor to probe extremely dilute analytes in a reasonable time frame[15]. Recent efforts towards this goal have primarily involved the fabrication of metallic electrodes at the nanopore surface to induce an electrical field[16,17]. Yet, to date, there has been no experimental report of *in situ* optoelectrical manipulation of high-density surface charge in nanopores or other nanoscale sensors.

We show here that an off-the-shelf, low-power visible laser beam can be used to directly manipulate the surface charge of a solid-state nanopore. The ability to dynamically increase surface charge has three immediate useful consequences. First, it allows the translocation speed of DNA to be tuned without chemically modifying the nanopore surfaces or altering the buffer properties. Second, it can be used to reliably unblock clogged nanopores, keeping them functional over prolonged periods of time. Third, it permits the detection of extremely low-molecular-weight proteins, which are otherwise nearly invisible to the resistive pulse sensing technique.

The photoconductive phenomenon in solid-state nanopores

A silicon nitride membrane containing a single nanopore was scanned in a custom-made confocal microscope with a tightly focused green laser (532 nm), as illustrated in Fig. 1a. The continuously recorded ionic current I flowing through the pore at a fixed voltage shows an increase when the laser spot overlaps with the nanopore location. Figure 1b illustrates this effect with an intensity surface plot of the ionic current I flowing through this pore as a function of laser spot position. A linescan through the image reveals a clear symmetric peak in the ionic current, more than double the baseline current level (full-width at half-maximum (FWHM) of ~500 nm; Fig. 1b, right panel).

This effect is evident in all tested pores (diameters of 4–20 nm), even for laser powers of just a few milliwatts. Although a tightly focused infrared laser at high power (~1 W) can produce a small increase in current by locally heating the solution[18], laser-induced heating can be ruled out here for two reasons: (1) the electromagnetic absorption of water at 532 nm is extremely small[19] and (2) the laser powers used in our experiments are only a few milliwatts. A temperature increase of ~35 K would be required to produce the observed increase in I, yet heating is estimated to account for a mere 0.005 K per mW of focused light based on measurements performed at 800 nm (ref. 20). We thus conclude that direct interaction of light with silicon nitride must cause this increase in the ion current via a photoconductive effect.

Permanent nanopore blocking by small molecules, tiny air bubbles or other nanoscale particulates is a common limitation

[1]Department of Biomedical Engineering, Boston University, Boston, Massachusetts 02215, USA, [2]Department of Biomedical Engineering, The Technion – Israel Institute of Technology, Haifa, Israel 32000, [3]Department of Electrical and Computer Engineering, Boston University, Boston, Massachusetts 02215, USA. *e-mail: ameller@bu.edu

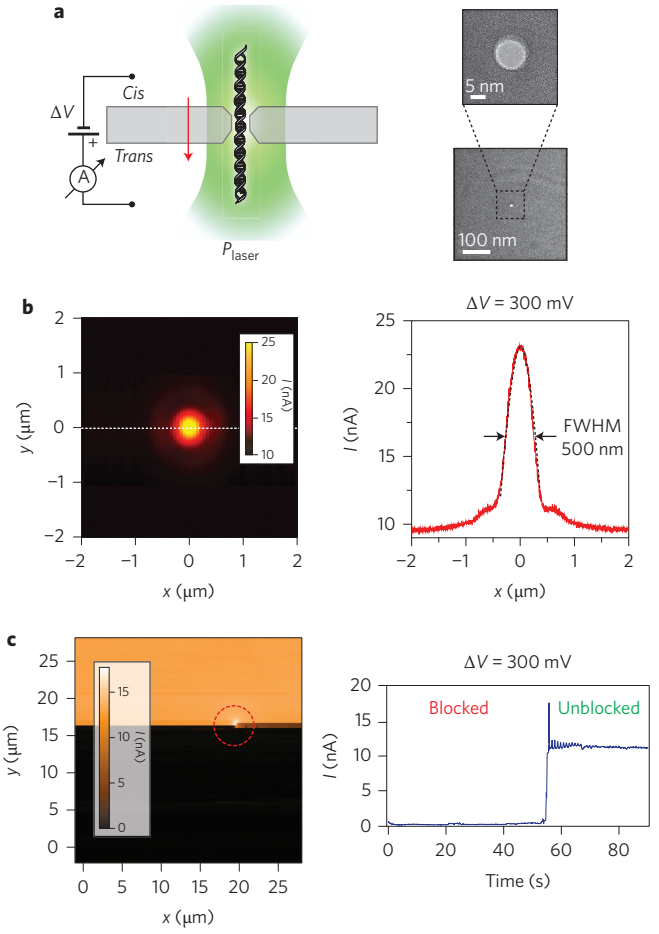

Figure 1 | The photoconductive effect in solid-state nanopores. a, Cartoon illustrating the optical nanopore set-up. A solid-state nanopore is positioned at a laser beam focus by a nanopositioner, and the ion current flowing through the pore is measured before and during translocation of DNA molecules. Inset: high-resolution transmission electron micrographs of a typical pore (diameter, 10 nm). **b**, Left: surface plot showing nanopore ionic current enhancement as a 10 mW focused laser beam ($\lambda = 532$ nm) scans the $4 \times 4\ \mu m^2$ SiN membrane at $1\ \mu m\ s^{-1}$. When the focused beam reaches the nanopore it produces a significant increase in measured current (2.4-fold increase for this pore). Right: line profile through $y = 0$, fitted using a Gaussian function with a FWHM of ~500 nm, consistent with the diffraction limit. **c**, Clearing a blocked solid-state nanopore with light. Left: a 5 mW laser intensity raster scan of the entire SiN window ($30 \times 30\ \mu m^2$, lower left to top right). The colour map represents the current flowing through the pore at $\Delta V = 300$ mV. As soon as the laser beam overlaps with the nanopore location, it clears the pore and, thereafter, the ionic current stabilizes at the open-pore level of 12 nA. Right: time trace of I during the laser scan.

for nanopore sensors, severely reducing their functional lifetime. In some cases, a series of electrical pulses will clear the pore[21], but often the system must be disassembled and recleaned. We find that in many of these cases a short exposure to a ~5 mW focused laser beam will immediately clear the nanopore. Figure 1c (left) shows a raster scan (bottom left to top right) of a fully blocked nanopore ($I \approx 0$ at $V = +300$ or -300 mV). As soon as the laser beam reaches the nanopore location, the pore is cleared. Thereafter, I stabilizes at the open-pore level of 12 nA. This is shown chronologically (Fig. 1c, right) as a time trace of I during the laser scan. We have found that light-induced nanopore unblocking is a highly robust and efficient tool to extend the functional lifetime of solid-state nanopores from a few hours to several days, as detailed in Supplementary Section 11.

Light-induced retardation of DNA and proteins

Over 1,000 translocation events of 10 kbp DNA were acquired in a nanopore (5.4 nm) in the dark (laser power $P = 0$). At $t = 150$ s, the laser radiation was switched on ($P = 2$ mW, pre-aligned with nanopore) as the software continued to record translocation events. Representative events before, during and after illumination are shown in Fig. 2a. Three features are immediately apparent: (1) the open-pore current (I_O) and the current during translocation (I_B) both increase when the laser is turned on; (2) the average event amplitude $\Delta I = I_O - I_B$ remains at the same level of 0.78 ± 0.10 nA under dark or light conditions; and (3) the mean event dwell-time t_D increases by a factor of ~10 under illumination compared with dark conditions. These features are illustrated in Fig. 2b, which shows I_O and ΔI as a function of time throughout the experiment (top panel). A 150-event running window average over all translocations (bottom panel) indeed shows a tenfold increase in the translocation time from ~1 ms to ~10 ms under laser illumination. We define the retardation factor (RF; here 10) as the increase in mean translocation time under laser light relative to darkness. Upon switching off the laser illumination at $t = 360$ s, I_O returns to the base level (3.6 nA) and the mean translocation dwell time is restored to ~1 ms, suggesting that this effect is completely reversible. This experiment was repeated for nanopores of various sizes, and in all cases we observed a marked retardation of translocation time under laser illumination (see Supplementary Section 2 for analysis).

We next tested the photoconductive effect for analytes other than DNA. Previous studies have sensed proteins such as bovine β-lactoglobulin or avidin[13,22] in solid-state nanopores, and antibodies such as anti-biotin Fab fragments or anti-biotin in lipid-coated nanopores[23]. However, the detection of small proteins ($M_w < 10$ kDa) in their native state remains a major challenge, because these proteins translocate through the pore too quickly to produce a resolvable signal given current bandwidth limitations[24].

We selected ubiquitin ($M_w \approx 8.5$ kDa; diameter, 4 nm) as a representative small protein, relevant to a broad range of biological processes[25], to demonstrate that the photoconductive effect can slow small protein translocations and enable their detection and characterization. Under dark conditions, purified wild-type ubiquitin (Supplementary Section 7) translocating through a ~5 nm pore yielded sporadic, brief downward spikes (red trace, Fig. 2c). The dwell time of these spikes was estimated to be <12 μs, but neither this nor the current amplitude of ubiquitin translocations could be accurately determined due to bandwidth constraints, even at 100 kHz (ref. 26), suggesting that the true translocation dwell time of these proteins is shorter than estimated.

Laser illumination of the same nanopore at $P = 4$ mW resulted in a marked increase in both the frequency and average dwell time of detected ubiquitin events (blue trace, Fig. 2c). The average translocation time increased by at least two orders of magnitude, allowing full characterization of both amplitude and dwell times for ubiquitin translocations. The increase in event rate under illumination may be attributed to events that were previously undetectable under dark conditions due to bandwidth limitations. As with DNA translocations, this effect was completely reversible.

A typical dwell time distribution and fractional blockade current I_B for illuminated ubiquitin translocations are shown in Fig. 2c ($N > 500$). Two prominent timescales are observed for ubiquitin translocation (340 ± 5 and 890 ± 70 μs), as well as two peaks in the blockade currents (0.88 and 0.78), approximated by a sum of two Gaussians. We hypothesize that the two peaks observed in these distributions may be associated with different orientations of the asymmetric 'mushroom-like' ubiquitin (Fig. 2c, inset) during

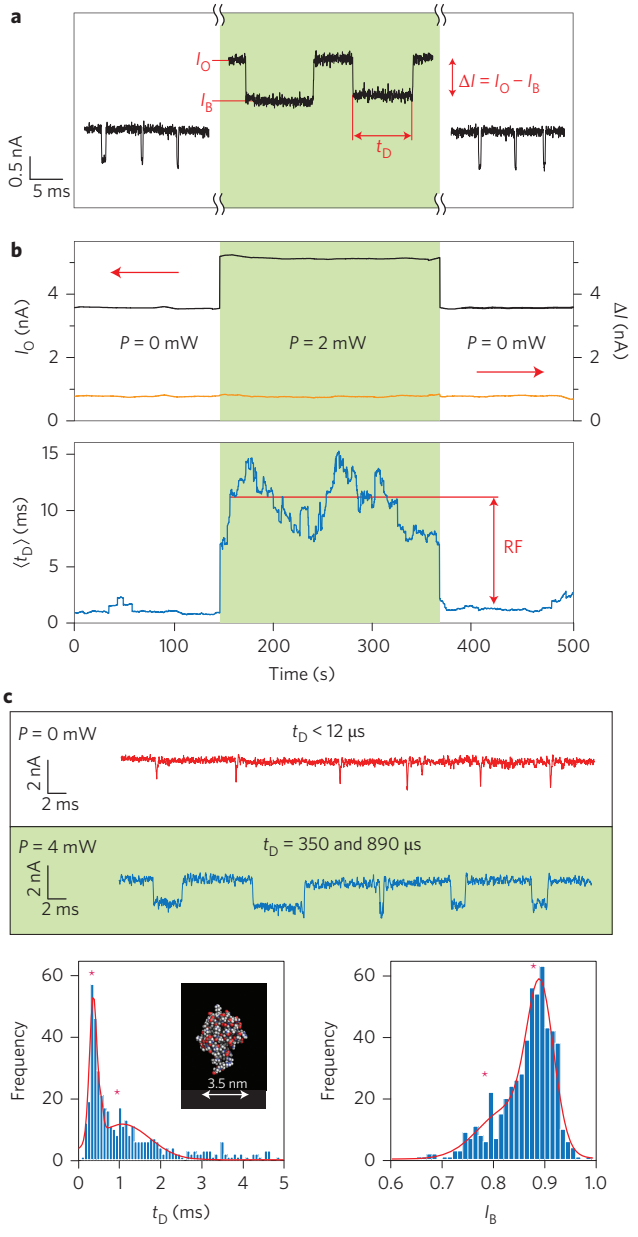

Figure 2 | Slowing down DNA and protein translocation speed with light. **a**, Representative translocation events with and without illumination, showing the increase in I_O, I_B and t_D. **b**, Time traces showing the open-pore current I_O, the blocked current amplitude ΔI (top panel) and the mean translocation time $\langle t_D \rangle$ (lower panel). The net effect of the laser illumination is to increase I_O and t_D while keeping ΔI constant. All data points in $\langle t_D \rangle$ represent a running average over 150 translocation events, initialized at the moment the laser is switched on/off. RF is defined as the mean t_D in light divided by the mean t_D in darkness. In this example, a factor of ~10 is obtained with $P = 2$ mW. **c**, Detection of the small-molecular-weight protein ubiquitin in its native state using a 5 nm nanopore, enabled by illumination of the chip with laser light. Typical translocation time traces are shown at $P = 0$ (red) and $P = 4$ mW (blue). With $P = 4$ mW we observe at least two orders of magnitude increase in the dwell times of the events. A typical translocation time distribution and fractional blockade current (I_B) of the ubiquitin under 4 mW of focused light are shown at the bottom ($N > 500$). Under these conditions, we typically observe two prominent timescales for ubiquitin translocation (340 ± 5 µs and 890 ± 70 µs), as well as two peaks in the blockade currents (0.88 and 0.78), approximated by a sum of two Gaussians (red lines). Inset: cartoon of the crystallographic structure of wild-type human ubiquitin (PDB 1d3z).

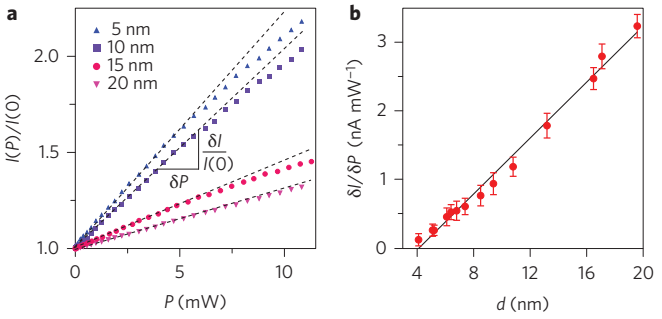

Figure 3 | Ionic current enhancement as a function of laser power and pore diameter. a, Plots of ionic current enhancement $I(P)/I(0)$ as a function of laser power for 5, 10, 15 and 20 nm diameter pores, as indicated. **b**, Pore response to light, $\delta I/\delta P$, obtained from linear fits to plots of $I(P)$, as a function of pore diameter. The dependence on pore size of the current enhancement shown in **a** and the pore response to light shown in **b** suggest that the origin of the photoconductance effect arises from the surface of the pore (that is, the pore walls) and not its volumetric content.

translocation. This hypothesis is consistent with previous reports for other protein–DNA complexes[27,28].

Light-induced modulation of electroosmotic flow

To elucidate the physical origin of light-induced retardation of translocation, we first characterized the pore current I at varying laser intensity P for a range of nanopore sizes (4–20 nm diameter, d). Figure 3a displays ionic current enhancement ($I(P)/I(0)$) for four representative pores ($d = 5$, 10, 15, 20 nm). In all cases I is linear for $P < 5$ mW, above which I deviates slightly from linearity. Linear fits for $P < 5$ mW characterize the response of each pore to light as the initial slope $\delta I/\delta P$. A plot of $\delta I/\delta P$ as a function of diameter for 14 pores (4–20 nm) exhibits a clear linear dependence on d (Fig. 3b). This suggests that when the SiN_x thickness L and nanopore drilling conditions are maintained, the pores' response to light per surface area (πdL) is a constant. From Fig. 3b we obtain a value of 2.2×10^{-3} nA mW^{-1} nm^{-2}.

The linear dependence of $\delta I/\delta P$ on nanopore diameter suggests that photoconductance current enhancement is a surface phenomenon rather than a volumetric one (which would exhibit $\propto d^2$ dependence). Solid-state nanopores possess weak surface charge, which can dominate pore conductivity at salt concentrations lower than ~100 mM (refs 29–31). However, it has been theorized that high charge densities on nanopore walls can affect electrical conductivity, even under high salt conditions[32,33]. Surface charges induce a diffuse double layer containing an excess of oppositely charged ions, of thickness comparable to the Debye screening length κ^{-1}. Ionic current is enhanced by the electrical double layer in two ways: (1) by creating a local imbalance of counter ions within κ^{-1}, which (2) drags water molecules with its motion, creating an electroosmotic flow (EOF) that in turn pulls along additional current (Fig. 4a). The total ionic current for a nanopore with a charged surface is

$$I = I_{bulk} + I_{DL} + I_{EOF} \quad (1)$$

where I_{bulk} is the current due to ions outside the electrical double layer, I_{DL} is the current due to ions forming the double layer, and I_{EOF} is the current due to net water flow induced by the net movement of ions within the double layer. I_{EOF} is proportional to the product of the flow velocity field and the net charge density $\rho(r)$, which is only non-zero within κ^{-1}. For small κ^{-1} compared to the pore diameter, (that is, $\kappa^{-1} \approx 0.3$ nm at 1 M KCl at 21 °C), only I_{bulk} scales with cross-sectional area ($I_{bulk} \propto \pi d^2$) whereas I_{DL} and I_{EOF} scale with circumference ($I_{DL}, I_{EOF} \propto \pi d\kappa^{-1}$). Thus,

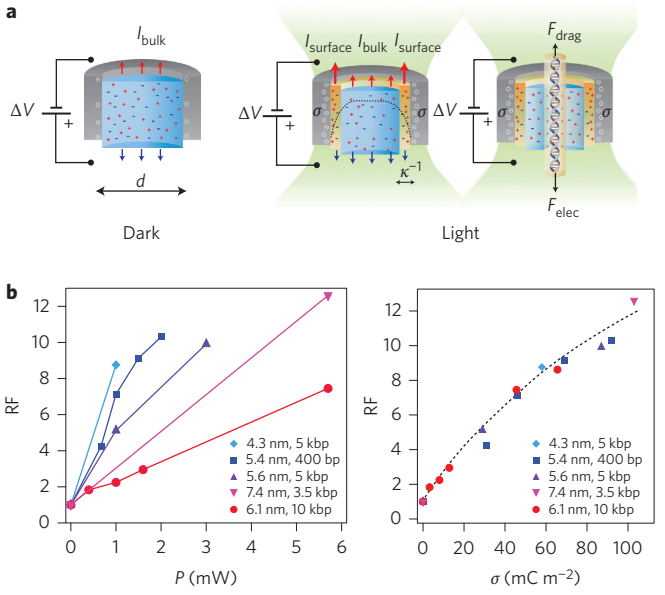

Figure 4 | Light-induced surface charge density modulates the EOF and DNA translocation speed. a, Cartoons showing the bulk and surface ionic current terms discussed in the text, and the origin of the EOF acting to retard the DNA translocation for the same nanopore in darkness (left) and under laser illumination (right). Here, $I_{surface} = I_{DL} + I_{EOF}$ (equation (1)). **b**, Left: RF as a function of laser intensity measured for different nanopore sizes, 4.3, 5.4, 5.6, 6.1 and 7.4 nm and DNA lengths, 400 bp, 3.5 kbp, 5 kbp and 10 kbp. Each data point was calculated from at least 1,000 events per laser intensity. Right: RF as a function of nanopore surface charge density calculated using the open-pore current versus laser intensity for each pore (equations (2)). Remarkably, all data points collapse onto a single curve, regardless of DNA length or nanopore diameter.

surface charges can, in principle, explain increased I as well as its linear scaling with d. Moreover, if the analyte remains mostly within the bulk pore volume where there is no charge imbalance, κ^{-1} distance away from the pore walls, we expect ΔI to be independent of surface charge, and thus independent of P. This is consistent with our observations (Fig. 2).

Previous theoretical work has predicted that surface charge on a nanopore will affect (1) translocation times[10,11] and (2) polymer capture rate[9,34]. A negatively charged nanopore produces an EOF towards the cathode (upper side, Fig. 4a), increasing the drag on a negatively charged translocating polymer, resulting in longer translocation times and reduced polymer capture rates. Conversely, positive surface charges would enhance the capture rate and reduce translocation times. Our results (Fig. 2) indicate that the RF for DNA translocation grows with laser intensity. Moreover, the DNA capture rate was reduced by 30%, from 11 s^{-1} to 8 s^{-1}, for 2 mW of laser light (Supplementary Section 2). These observations lead us to hypothesize that visible light can induce negative surface charges on silicon nitride, which in turn slows DNA translocation via the drag created by EOF moving in the opposite direction to the DNA.

To validate this hypothesis we approximate that for low laser powers the surface charge density σ grows linearly with laser intensity, such that $\sigma = \gamma P$ where γ is the photoreactivity of the pore (C m^{-2} W^{-1}). The total ionic current I can be obtained as a function of surface charge density using the following three individual contributions (see Supplementary Section 4 for full derivation): (1) I_{bulk}, the electrophoretic movement of each ion species through the nanopore; (ii) I_{DL}, which may be determined from the net charge distribution ρ for a given wall potential, derived analytically from the Poisson–Boltzmann equation and from the Boltzmann distribution, assuming a cylindrical nanopore and using the Debye–Hückel approximation[9–11]; (3) I_{EOF}, which is a product of ρ and the EOF velocity profile described by the Navier–Stokes equation. The Grahame equation may be substituted to give σ as a function of wall potential[35]. The contributions to the ion current are

$$I_{bulk} \approx en_{KCl}(\mu_K + \mu_{Cl})\frac{\pi d^2}{4L}\Delta V \quad (2.1)$$

$$I_{DL} \approx \frac{2\pi d\varepsilon\kappa\mu_K}{L}\sinh\left(\frac{\beta e\gamma P}{2\kappa\varepsilon}\right)\Delta V \quad (2.2)$$

$$I_{EOF} \approx \frac{2\pi d\kappa\varepsilon^2}{L\eta\beta^2 e^2}\left[\sinh^{-1}\left(\frac{\beta e\gamma P}{2\kappa\varepsilon}\right)\right]^2\Delta V \quad (2.3)$$

for elementary charge e, permittivity of aqueous solution ε, parameter $\beta = 1/k_BT$ (k_B, Boltzmann constant; T, absolute temperature), pore length L, applied voltage clamp ΔV, and solution viscosity η. The number density of potassium or chloride ions is n_{KCl}, with electrophoretic mobilities μ_K and μ_{Cl} (see Supplementary Section 4 for numerical values). Nanopore diameter d can be determined from transmission electron microscopy (TEM) images, enabling a quantitative estimation of the nanopore photoreactivity γ via equations (2) (Supplementary Fig. 7). We also measured the dependence of I on KCl concentration (0.01–1 M) at different P and found it consistent with the model (Supplementary Fig. 8).

Additional DNA translocations were performed using a range of DNA lengths, nanopores and laser powers to determine the role of surface charge in slowing translocation speed. The results are summarized in Fig. 4b (left), where RF is plotted against P for five nanopores (4.3, 5.4, 5.6, 6.1 and 7.4 nm diameters) and four DNA lengths (0.4, 3.5, 5 and 10 kbp). t_D was measured for more than 1,000 events per laser intensity, and the t_D histograms were fitted with exponential functions as previously described[26]. These measurements suggest that RF per mW of light varies widely with pore size and DNA length.

Fitting equations (2) as described above to obtain γ for each of the pores, we then transformed the DNA RF into surface charge density σ using the relationship $\sigma = \gamma P$. Remarkably, all data points collapse onto a single curve (Fig. 4b, right). Thus, light-induced slowing is dependent only on the induced surface charge density σ. Controlling the RF value can be achieved either by selecting a highly optically reactive pore (high γ) under low laser intensity, or using a less optically reactive pore under higher laser intensity.

Photoreactivity depends on e-beam exposure

Drilling nanopores in SiN_x with an electron beam reduces the N/Si ratio around the pore due to preferential ablation of N atoms[36]. Moreover, the principal defects in silicon-rich chemical vapour deposition-derived amorphous SiN_x materials are Si dangling bonds, which can trap electrons or holes to become charged[37–39]. When the N/Si ratio approaches 0.8, the bandgap is within visible-light energies[39,40]. When the N/Si ratio of the material surrounding the pore is low enough, we propose that visible light can excite electrons from the ground state across the bandgap, trapping them in Si dangling bonds[41]. Eventually, trapped electrons would recombine with holes, but a high density of arriving photons could maintain a steady state of negatively charged Si dangling bonds, creating a net surface charge density.

We TEM-drilled four additional nanopores, all with similar diameters, in a freshly deposited SiN_x membrane. Two were

exposed to the electron beam for 60 s, and two were exposed for 500 s, producing different local N/Si stoichiometry (Supplementary Section 8)[42]. As expected, the pores drilled with a low electron beam dose had relatively low photoreactivity ($\gamma = 27$ C m^{-2} W^{-1}), whereas the pores exposed to a high electron beam dose had much higher photoreactivity ($\gamma = 70$ C m^{-2} W^{-1}), establishing a direct correlation between electron beam dosage and optical reactivity.

Conclusions

We have shown that just a few milliwatts of visible laser light focused on a nanopore can induce surface charge densities up to ~1 C m^{-2}, much larger than the weak native charge of SiN_x. Increased σ produces net charge near the pore walls, which, under external voltage, creates an electroosmotic flow moving in opposition to an anionic translocating molecule. This flow slows translocating DNA and proteins, allowing the detection and characterization of small analytes such as ubiquitin. Previous approaches to slowing analyte translocation have introduced permanent modifications to the nanopore walls, inducing stronger interactions of analytes with the pore surface during translocation[13,23,43,44]. By contrast, the optoelectronic effect allows completely reversible, *in situ* control of σ and translocation speed without permanently altering the surface properties of the nanopore or buffer[45,46]. This is particularly useful for the detection and characterization of molecules in their native form. Moreover, ultrafast tuning of surface charge by light completely decouples the capture process from subsequent translocation. Solid-state lasers, as well as other light sources, can be readily switched on/off in submicrosecond timescales, and hence induce current jumps in the nanopores within milliseconds (Supplementary Section 3). The dynamic range of the photoconductive effect is determined by local N/Si stoichiometry, which in turn depends on electron beam exposure during nanopore drilling. We predict that this method will facilitate a broad range of emerging nanopore sensing applications, including genotyping using peptide nucleic acid (PNA) probes[47] and quantification of epigenetic markers[48,49].

Ultrafast and reversible modulation of surface charge is fundamentally important for the development of novel nanosensors. By exploiting the intrinsically high sensitivity of the nanopore ionic current to small modulations of surface charge, we were able to explore and characterize a new optoelectronic effect, model the increase in electric conductance under visible laser illumination, and propose an underlying mechanism. We have shown here three useful applications for the technique: (1) clearing blocked nanopores and thus significantly extending their useful lifetime; (2) slowing and tuning the translocation speed of DNA; and (3) detecting and characterizing translocation events of very small proteins such as ubiquitin. Together, these milestones broaden the range of molecules that can be probed by solid-state nanopores, enhance nanopore sensitivity, and extend the lifetime and throughput of individual pores.

Methods

Nanopores were drilled on low-stress (Si-rich), amorphous low pressure chemical vapour-deposited SiN_x membranes (30 nm thick). Chips were then cleaned using Piranha solution and kept in water until mounted on the Teflon holder, giving two independent chambers connected by the nanopore and filled with an electrolytic solution (1 M KCl, 20 mM Tris, pH 8.0, 21 °C). A pair of Ag/AgCl electrodes was used to apply an electrostatic potential difference across the chambers separated by the insulating SiN_x membrane. The resulting ionic current through the nanopore was recorded using a patch-clamp amplifier (Axopatch 200B, Molecular Devices Corporation). The entire apparatus was shielded from external electromagnetic noise by a Faraday cage. The electrical readout from the amplifier was filtered with a 10 kHz or with a 100 kHz low-pass Bessel filter and digitized using a 16 bit analog-to-digital card (National Instruments) controlled by a custom-written LabView (National Instruments) program (see Supplementary Section 10 for a detailed diagram of the apparatus).

The nanochip was secured to a closed-loop nanopositioner (Physik Instrumente) with subnanometre accuracy, also controlled by the LabView program. The nanopositioner was mounted in a custom-built confocal set-up in order to illuminate the nanopore with a focused laser beam. A 532 nm line from a laser diode (New Focus) was cleaned by a Glan-Thompson polarizer (Thorlabs), with the final power adjusted on demand by a half-wave plate mounted on a motorized rotating holder. This resulted in a final dynamic range of 2 μW to 17 mW with 500 intermediate values. The laser beam was expanded to completely fill the back aperture of a ×60, 1.2 NA water immersion objective (Olympus UPlanApo). The emission side contained a long-pass filter (Chroma HQ560LP) to remove any elastically scattered light, followed by a focusing lens and a charge-coupled device camera (Thorlabs DC111) for direct visualization of the membrane.

Received 11 January 2013; accepted 26 September 2013; published online 3 November 2013

References

1. Zhang, X., Ju, H. & Wang, J. *Electrochemical Sensors, Biosensors and their Biomedical Applications* (Elsevier, 2008).
2. Venkatesan, B. M. & Bashir, R. Nanopore sensors for nucleic acid analysis. *Nature Nanotech.* **6,** 615–624 (2011).
3. Tegenfeldt, J. O. *et al.* The dynamics of genomic-length DNA molecules in 100-nm channels. *Proc. Natl Acad. Sci. USA* **101,** 10979–10983 (2004).
4. Pang, P., He, J., Park, J., Krstic, P. S. & Lindsay, S. Origin of giant ionic currents in carbon nanotube channels. *ACS Nano* **5,** 7277–7283 (2011).
5. Guan, W., Fan, R. & Reed, M. A. Field-effect reconfigurable nanofluidic ionic diodes. *Nature Commun.* **2,** 506 (2011).
6. Dekker, C. Solid-state nanopores. *Nature Nanotech.* **2,** 209–215 (2007).
7. Healy, K. Nanopore-based single-molecule DNA analysis. *Nanomedicine* **2,** 459–481 (2007).
8. Wanunu, M. & Meller, A. in *Laboratory Manual on Single Molecules* (eds Ha, T. & Selvin, P.) 395–420 (Cold Spring Harbor Press, 2008).
9. Wong, C. T. A. & Muthukumar, M. Polymer capture by electro-osmotic flow of oppositely charged nanopores. *J. Chem. Phys.* **126,** 164903 (2007).
10. He, Y., Tsutsui, M., Fan, C., Taniguchi, M. & Kawai, T. Controlling DNA translocation through gate modulation of nanopore wall surface charges. *ACS Nano* **5,** 5509–5518 (2011).
11. Kejian, D., Weimin, S., Haiyan, Z., Xianglei, P. & Honggang, H. Dependence of zeta potential on polyelectrolyte moving through a solid-state nanopore. *Appl. Phys. Lett.* **94,** 014101 (2009).
12. Van Dorp, S., Keyser, U. F., Dekker, N. H., Dekker, C. & Lemay, S. G. Origin of the electrophoretic force on DNA in solid-state nanopores. *Nature Phys.* **5,** 347–351 (2009).
13. Firnkes, M., Pedone, D., Knezevic, J., Döblinger, M. & Rant, U. Electrically facilitated translocations of proteins through silicon nitride nanopores: conjoint and competitive action of diffusion, electrophoresis, and electroosmosis. *Nano Lett.* **10,** 2162–2167 (2010).
14. Iqbal, S. M. & Bashir, R. (eds) *Nanopores, Sensing and Foundamental Biological Interactions* (Springer, 2011).
15. Wanunu, M., Morrison, W., Rabin, Y., Grosberg, A. Y. & Meller, A. Electrostatic focusing of unlabelled DNA into nanoscale pores using a salt gradient. *Nature Nanotech.* **5,** 160–165 (2010).
16. Nam, S-W., Rooks, M. J., Kim, K-B. & Rossnagel, S. M. Ionic field effect transistors with sub-10 nm multiple nanopores. *Nano Lett.* **9,** 2044–2048 (2009).
17. Jiang, Z. & Stein, D. Charge regulation in nanopore ionic field-effect transistors. *Phys. Rev. E* **83,** 031203 (2011).
18. Keyser, U. F. *et al.* Nanopore tomography of a laser focus. *Nano Lett.* **5,** 2253–2256 (2005).
19. Svoboda, K. & Block, S. M. Biological applications of optical forces. *Annu. Rev. Biophys. Biomol. Struct.* **23,** 247–285 (1994).
20. Peterman, E. J. G., Gittes, F. & Schmidt, C. F. Laser-induced heating in optical traps. *Biophys. J.* **84,** 1308–1316 (2003).
21. Beamish, E., Kwok, H., Tabard-Cossa, V. & Godin, M. Precise control of the size and noise of solid-state nanopores using high electric fields. *Nanotechnology* **23,** 405301 (2012).
22. Talaga, D. S. & Li, J. Single-molecule protein unfolding in solid state nanopores. *J. Am. Chem. Soc.* **131,** 9287–9297 (2009).
23. Yusko, E. C. *et al.* Controlling protein translocation through nanopores with bio-inspired fluid walls. *Nature Nanotech.* **6,** 253–260 (2011).
24. Plesa, C. *et al.* Fast translocation of proteins through solid state nanopores. *Nano Lett.* **13,** 658–663 (2013).
25. Welchman, R. L., Gordon, C. & Mayer, R. J. Ubiquitin and ubiquitin-like proteins as multifunctional signals. *Nature Rev. Mol. Cell. Biol.* **6,** 599–609 (2005).
26. Wanunu, M., Sutin, J., McNally, B., Chow, A. & Meller, A. DNA translocation governed by interactions with solid state nanopores. *Biophys. J.* **95,** 4716–4725 (2008).
27. Soni, G. V. & Dekker, C. Detection of nucleosomal substructures using solid-state nanopores. *Nano Lett.* **12,** 3180–3186 (2012).
28. Raillon, C. *et al.* Nanopore detection of single molecule RNAP–DNA transcription complex. *Nano Lett.* **12,** 1157–1164 (2012).

29. Ho, C. *et al.* Electrolytic transport through a synthetic nanometer-diameter pore. *Proc. Natl Acad. Sci. USA* **102,** 10445–10450 (2005).
30. Hoogerheide, D. P., Garaj, S. & Golovchenko, J. A. Probing surface charge fluctuations with solid-state nanopores. *Phys. Rev. Lett.* **102,** 256804 (2009).
31. Smeets, R. *et al.* Salt dependence of ion transport and DNA translocation through solid-state nanopores. *Nano Lett.* **6,** 89–95 (2006).
32. Chen, Y., Ni, Z. & Wang, G. Electroosmotic flow in nanotubes with high surface charge densities. *Nano Lett.* **8,** 42–48 (2008).
33. Plecis, A., Schoch, R. B. & Renaud, P. Ionic transport phenomena in nanofluidics: experimental and theoretical study of the exclusion-enrichment effect on a chip. *Nano Lett.* **5,** 1147–1155 (2005).
34. He, Y., Tsutsui, M., Fan, C., Taniguchi, M. & Kawai, T. Gate manipulation of DNA capture into nanopores. *ACS Nano* **5,** 8391–8397 (2011).
35. Behrens, S. H. & Grier, D. G. The charge of glass and silica surfaces. *J. Chem. Phys.* **115,** 6716–6721 (2001).
36. Wu, M. *et al.* Control of shape and material composition of solid-state nanopores. *Nano Lett.* **9,** 479–484 (2009).
37. Deshpande, S. V. & Gulari, E. Optical properties of silicon nitride films deposited by hot filament chemical vapor deposition. *J. Appl. Phys.* **77,** 6534–6541 (1995).
38. Moustakas, T. D. The role of extended defects on the performance of optoelectronic devices in nitride semiconductors. *Phys. Status Solidi (a)* **210,** 169–174 (2012).
39. Robertson, J., Warren, W. L. & Kanicki, J. Nature of the Si and N dangling bonds in silicon nitride. *J. Non-Cryst. Solids* **187,** 297–300 (1995).
40. Robertson, J. & Powell, M. J. Gap states in silicon nitride. *Appl. Phys. Lett.* **44,** 415–417 (1984).
41. Singh, R., Molnar, R. J., Unlu, M. S. & Moustakas, T. D. Intensity dependence of photoluminescence in gallium nitride thin films. *Appl. Phys. Lett.* **64,** 336–338 (1994).
42. Wu, M. Y., Krapf, D., Zandbergen, M., Zandbergen, H. & Batson, P. E. Formation of nanopores in a SiN/SiO_2 membrane with an electron beam. *Appl. Phys. Lett.* **87,** 113106 (2005).
43. Venkatesan, B. M., Shah, A. B., Zuo, J-M. & Bashir, R. DNA sensing using nanocrystalline surface-enhanced Al_2O_3 nanopore sensors. *Adv. Funct. Mater.* **20,** 1266–1275 (2010).
44. Anderson, B. N., Muthukumar, M. & Meller, A. pH tuning of DNA translocation time through organically functionalized nanopores. *ACS Nano* **7,** 1408–1414 (2013).
45. Fologea, D., Uplinger, J., Thomas, B., McNabb, D. S. & Li, J. Slowing DNA translocation in a solid-state nanopore. *Nano Lett.* **5,** 1734–1737 (2005).
46. Kowalczyk, S. W., Wells, D. B., Aksimentiev, A. & Dekker, C. Slowing down DNA translocation through a nanopore in lithium chloride. *Nano Lett.* **12,** 1038–1044 (2012).
47. Singer, A., Rapireddy, S., Ly, D. H. & Meller, A. Electronic barcoding of a viral gene at the single-molecule level. *Nano Lett.* **12,** 1722–1728 (2012).
48. Shim, J. *et al.* Detection and quantification of methylation in DNA using solid-state nanopores. *Sci. Rep.* **3,** 1389 (2013).
49. Wanunu, M. *et al.* Discrimination of methylcytosine from hydroxymethylcytosine in DNA molecules. *J. Am. Chem. Soc.* **133,** 486–492 (2011).

Acknowledgements

The authors acknowledge support for this work from the National Institutes of Health (NHGRI grant no. R01 HG-005871), from the Marie Curie People award (GA-2010-277060, ERC) and from the Israeli Centers of Research Excellence (I-CORE) programme (Center #1902/12). The authors also thank the staff at the Harvard University Center for Nanoscale Sciences (CNS) and the Technion Electron Microscopy Center for dedicated support.

Author contributions

N.D.F. and A.M. conceived and designed the experiments. N.D.F., D.B. and T.G. performed the experiments. A.S. drilled all pores. N.D.F., A.S., D.B., T.G. and A.M. analysed the data. N.D.F., T.D.M. and A.M. developed the model. N.D.F., A.S., D.B., T.G., T.D.M. and A.M. co-wrote the paper.

Additional information

Supplementary information is available in the online version of the paper. Reprints and permissions information is available online at www.nature.com/reprints. Correspondence and requests for materials should be addressed to A.M.

Competing financial interests

The authors declare no competing financial interests.